

Vibrational Relaxation and Fragmentation in Icosahedral $(\text{Ar}_2^+)\text{Ar}_{12}$ Clusters

Jongbaik Ree,* Yoo Hang Kim,[†] and Hyung Kyu Shin[‡]

Department of Chemistry Education, Chonnam National University, Gwangju 500-757, Korea. *E-mail: jbree@jnu.ac.kr

[†]Department of Chemistry, Inha University, Incheon 402-751, Korea

[‡]Department of Chemistry, University of Nevada, Reno, Nevada 89557, USA

Received March 6, 2014, Accepted May 28, 2014

A dynamics study of relaxation and fragmentation of icosahedral argon cluster with a vibrationally excited Ar_2^+ (ν) is presented. Local translation is shown to be responsible for inducing energy flow from the embedded ion to host atoms and fragmentation of the cluster consisting of various low frequency modes. The total potential energy of $(\text{Ar}_2^+)\text{Ar}_{12}$ is formulated using a building-up procedure of host-guest and host-host interactions. The time dependence of ion-to-host energy transfer is found to be tri-exponential, with the short-time process of ~ 100 ps contributing most to the overall relaxation process. Relaxation timescales are weakly dependent on both temperature (50-300 K) and initial vibrational excitation ($\nu = 1-4$). Nearly 27% of host atoms in the cluster with $\text{Ar}_2^+(\nu = 1)$ fragment immediately after energy flow, the extent increasing to $\sim 43\%$ for $\nu = 4$. The distribution of fragmentation products of $(\text{Ar}_2^+)\text{Ar}_{12} \rightarrow (\text{Ar}_2^+)\text{Ar}_n + (12-n)\text{Ar}$ are peaked around $(\text{Ar}_2^+)\text{Ar}_8$. The distribution of dissociation times reveals fragmentation from one hemisphere dominates that from the other. This effect is attributed to the initial fragmentation causing a sequential perturbation of adjacent atoms on the same icosahedral five-atom layer.

Key Words : Vibrational relaxation, Fragmentation, Icosahedral, Ar cluster

Introduction

The ions of inert gas clusters have been the subject of much research during the past decades both experimentally and theoretically.¹⁻¹⁹ These studies have focused on fragmentation,^{1,4,14-16} thermochemistry,⁵ ground-state geometries,^{3,6,11,13,17} interaction potential energies⁷⁻⁹ and energy transfer dynamics^{10,19} among others. Small to medium-size clusters occupy an intermediate position between gas and condensed phases. Such clusters with embedded guest (or impurity) molecules provide an attractive model system for studying the physical and chemical processes, such as solvent effects, evaporation, melting or vibrational relaxation.^{2,10,19} Many-body host-host and guest-host interactions induced by nonbonding interactions can lead to a potential energy surface with periodic local minima, which can influence the motions of guest molecules and the fragmentation of host atoms. Argon clusters provide a large enough space where a diatomic or small polyatomic molecule can be embedded to play its role on intra-cluster processes such as energy flow and subsequent fragmentation.

In this paper, we model a vibrationally excited Ar_2^+ ion embedded in an icosahedral argon cluster, $(\text{Ar}_2^+)\text{Ar}_{12}$, and study the energy flow from the ion to host atoms and the fragmentation process $(\text{Ar}_2^+)\text{Ar}_{12} \rightarrow (\text{Ar}_2^+)\text{Ar}_n + (12-n)\text{Ar}$. The contents are organized as follows. The Model and Methods section describes the environment of the ion embedded in the first solvation shell, formulation of Ar_2^+ intramolecular and Ar-Ar intramolecular potential functions and method of solving the equations of motion. The extents of energy flow and fragmentation are presented in the

Results and Discussion section followed by the Concluding Remarks section. Dynamics studies are carried out by integrating the equations of motion for 5000 clusters, which contain 60 000 host atoms and 10 000 atoms of the guest ion, over the temperature range of 50-300 K and initial vibrational excitation $\nu = 1-4$ of Ar_2^+ .

Model and Methods

Cluster Geometry. The host atoms in the icosahedral cluster $(\text{Ar}_2^+)\text{Ar}_{12}$ are numbered as in Figure 1, where the 6th and 12th atoms are at the axial positions on the Z axis. The diatomic ion Ar_2^+ is placed in parentheses. The $n = 1-5$ atoms are in the upper 5-atom layer at $\theta = 58^\circ$ and $\phi = 0, 72, \dots, 288^\circ$, respectively, whereas $n = 7-11$ are in the lower 5-atom layer at $\theta = 122^\circ$ and $\phi = 36, 108, \dots, 324^\circ$, respectively. Individual host atoms are identified as Ar(1), Ar(2), ..., Ar(12), respectively. Subscript numbers are reserved for cluster sizes in discussing fragmentation products; e.g., subscript 6 in $(\text{Ar}_2^+)\text{Ar}_6$ of $(\text{Ar}_2^+)\text{Ar}_n$, where $n = 1-12$. The two atoms of Ar_2^+ are identified with a subscript as $\text{Ar}_{\text{ion}(1)}$ and $\text{Ar}_{\text{ion}(2)}$ to distinguish them from host atoms Ar(n). A vibrationally excited Ar_2^+ embedded in the cluster interacts with 12 host atoms, while undergoing local translation (δ). In Figure 1, we take Ar(5) as an example and denote its displacement from its equilibrium position by q_5 ; see the shaded Ar(5). The instantaneous distance between Ar(5) and a nearest neighbor Ar(n) is $(d - q_5 + q_n)$ or in general, $(d - q_n + q_n)$ between n th and n' th atoms, where d is the equilibrium distance between the first-neighbors. The distance $(-q_n + q_n)$ represents the distortion of the $(\text{Ar}_2^+)\text{Ar}_{12}$ con-

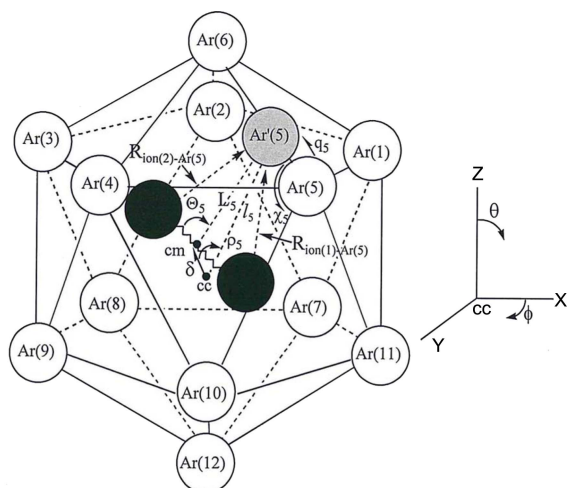


Figure 1. Numbering of host atoms and coordinate systems in icosahedral $(Ar_2^+)Ar_{12}$ around the cage center (*c.c.*) are shown. Each host atom is at one of 12 vertices. Interatomic distances and angles are defined. The displacement of the center-of-mass (*c.m.*) of Ar_2^+ is displaced from the *c.c.* by δ . A shaded circle is the displaced $Ar(5)$ from its equilibrium position by q_5 .

figuration from the regular icosahedron geometry, the distortion which can become particularly severe in the presence of an embedded guest. In addition to 24 ion-host (*ion-h*) atom interactions, the cluster consists of 30 first-neighbor, 30 second-neighbor and six third-neighbor host-host (*h-h*) interactions.

Interaction Potential Energy. The distances from $Ar'(5)$ to $Ar_{ion(1)}$ and $Ar_{ion(2)}$ are denoted by $R_{Ar(5)-ion(1)}$ and $R_{Ar(5)-ion(2)}$, respectively. These *ion-h* distances are

$$R_{Ar(n)-ion(1)} = \left[L_n^2 + \frac{1}{4}r^2 + crL_n \cos \Theta_n \right]^{1/2}, \quad n = 1-12 \quad (1)$$

where r is the instantaneous bond distance of Ar_2^+ and $c = -1$. The same expression with $c = 1$ is for $R_{Ar(n)-ion(2)}$. Here L_n is the distance between the center of mass (*c.m.*) of Ar_2^+ and n th host atom, $L_n = (\ell_n^2 + \delta^2 - 2\ell_n\delta\cos\rho_n)^{1/2}$ and $\ell_n = (\ell^2 + q_n^2 - 2\ell_nq_n\cos\chi_n)^{1/2}$ and $\ell = 3.892 \text{ \AA}$ represents the distance between the cluster center or cage center (*cc*) and the initial position of $Ar(5)$ or the radius of the present cluster.¹⁹ This distance forms a cage space large enough to embed Ar_2^+ , whose equilibrium bond distance is 2.4221 \AA .²⁰ The explicit forms of the angle Θ_n , defining the orientation of Ar_n in the cage are

$$\Theta_n = \arccos\{0.5257\cos\theta + 0.8506\sin\theta\cos[2(n-1)\pi/5 - \phi]\}$$

for $n = 1-5$

$$\Theta_n = \arccos\{0.5257\cos\theta - 0.8506\sin\theta\cos[\lambda\pi/5 - \phi]\}$$

for $n = 7-11$ and $\lambda = 1, 3, 5, 7, 9$.

For $n = 6$ and 12 , $\Theta_n = \theta$. The angle factors $\cos\rho_n$ and $\cos\chi_n$ in L_n are replaced by the orientation averaged values 0 and $1/2$, respectively.²¹

The total interaction energy needed to describe the dynamic processes taking place in the cluster $(Ar_2^+)Ar_{12}$ is a sum of the intramolecular potential of Ar_2^+ , host-host interactions, host oscillations and host-ion interactions including the

polarization contribution,

$$V(r, \theta, \phi, \delta, \{q\}) = V_{Ar_2^+}(r) + V_{h-h}(\{q\}) + V_{Ar}(\{q\}) + V_{ion-h}(r, \theta, \phi, \delta, \{q\}) \quad (2)$$

The first term is expressed in the Morse form

$$V_{Ar_2^+}(r) = D_e \{ \exp[(r_e - r)/a_{Ar_2^+}] - 2 \exp[(r_e - r)/2a_{Ar_2^+}] \} \quad (3)$$

where r_e is the equilibrium bond distance 2.4221 \AA ²⁰ and the exponential range parameter calculated from $a_{Ar_2^+} = (D_e/2\mu_{Ar_2^+})^{1/2}/\omega_{Ar_2^+}$, with $D_e = 1.3903 \text{ eV}$ ^{7,20} and $\omega_{Ar_2^+} = 307 \text{ cm}^{-1}$ ²² is 0.317 \AA . When the latter potential parameters are used, Eq. (3) is in close agreement with the observed and computationally determined energies.^{7,20,23}

The host-host interaction potential is

$$V_{h-h}(\{q\}) = 4\varepsilon \sum_{n,n'} \{ [d/(d - q_n + q_{n'})]^{12} - 2[d/(d - q_n + q_{n'})]^6 \} \quad (4)$$

where the summation is over all pair-wise interactions and the Lennard-Jones (LJ) constants are $\varepsilon = 143.224 \text{ K}$ (or 0.01234 eV) and $d = 3.757 \text{ \AA}$.^{24,25} For $n = 1$, the first-neighbors are $Ar(2)$, $Ar(5)$, $Ar(6)$, $Ar(7)$, $Ar(11)$, and the second-neighbors are $Ar(3)$, $Ar(4)$, $Ar(8)$, $Ar(10)$, $Ar(12)$, and the third-neighbor is $Ar(9)$. It is important to establish the range of distances, which best describe the present cluster environment embedded with Ar_2^+ . For a regular icosahedron with $\ell = 3.892 \text{ \AA}$, the nearest distance between the apex atoms is 4.092 \AA . In this expanded cluster, host atoms oscillate around their nearest equilibrium positions separated from their first-neighbors by 3.757 \AA . If we take a 4% displacement for each atom, the maximum and minimum distances between the atoms of the first-neighbor (or a dimer) are 4.057 and 3.456 \AA , respectively. Thus the apex distance 4.092 \AA in the expanded cluster creates a large enough shell area for the neighbors to move without suffering significant repulsive interactions. In the expanded cluster, the distance between the second-neighbors is 6.621 \AA , whereas that between the third-neighbors is $2\ell = 7.784 \text{ \AA}$.

We describe the oscillatory motion of each host atom around its equilibrium position in the form

$$V_{Ar}(\{q\})_{\text{host}} = D_{Ar} \sum_{n=1}^{12} [\exp(-q_n/a_{Ar}) - 2\exp(-q_n/2a_{Ar})] \quad (5)$$

where D_{Ar} measures the energy exerted by each neighbor, which we set equal to ε . The exponential range parameter is $a_{Ar} = (D_{Ar}/2m)^{1/2}/\omega_{Ar} = 0.298 \text{ \AA}$ with the dimer frequency 30.68 cm^{-1} for ω_{Ar} ^{26,27} and the reduced mass of m .

The dimer ion represented by Eq. (3) is quite stable ($D_e = 1.39 \text{ eV}$), but its interaction with host atoms is comparatively much weaker. The main contribution to the *ion-h* interaction will be the polarization energy of Ar in the field of Ar_2^+ . Thus the interaction of the ion with 12 host atom can be expressed as a sum of the neutral $Ar_{ion(1)-Ar}$ and $Ar_{ion(2)-Ar}$ interactions at the *ion-h* distances defined in Eq. (1) and the polarization energy at the *c.m.*-to-host distance:

$$\begin{aligned}
 V_{\text{ion-h}}(r, \theta, \phi, \delta, \{q\}) = & 4\varepsilon \sum_{n=1}^{12} [(d/R_{\text{Ar(n)-ion(1)}})^{12} \\
 & - 2(d/R_{\text{Ar(n)-ion(1)}})^6] + 4\varepsilon \sum_{n=1}^{12} [(d/R_{\text{Ar(n)-ion(2)}})^{12} \\
 & - 2(d/R_{\text{Ar(n)-ion(2)}})^6] - \sum_{n=1}^{12} [(\alpha_{\text{Ar}} e^2 / 4\pi\varepsilon_0) / 2L_n^4] \quad (6)
 \end{aligned}$$

where $\alpha_{\text{Ar}} = 1.64 \text{ \AA}^3$.²⁸ As the distances in Eq. (6) are dependent on the coordinates set $(r, \theta, \phi, \delta, \{q\})$, the *ion-h* energy determines the coupling of all motions in the cluster, thus playing a central role in the dynamics processes.

Potential Energy Surfaces. Figure 2(a) shows the rotational potential energy surface (PES) for $(\text{Ar}_2^+) \text{Ar}_{12}$. The five peaks (0.0189 eV) appearing at $\theta = 58^\circ$ are for the repulsive interactions of $\text{Ar}_{\text{ion(1)}}$ with the five upper-layer atoms located at the ϕ angle 72° -intervals. The maximum (0.0477 eV) at $\theta = 0^\circ$ is for the interaction of $\text{Ar}_{\text{ion(1)}}$ with the axial atom Ar(6), whereas that at $\theta = 180^\circ$ is for the interaction of $\text{Ar}_{\text{ion(2)}}$ with Ar(12). The five peaks fit nearly perfectly the 5-fold symmetry expression $V_h = \frac{1}{2}E_h(1 + \cos 5\phi)^{1/2}$, indicating that the rotational motion in the ϕ -direction is hindered

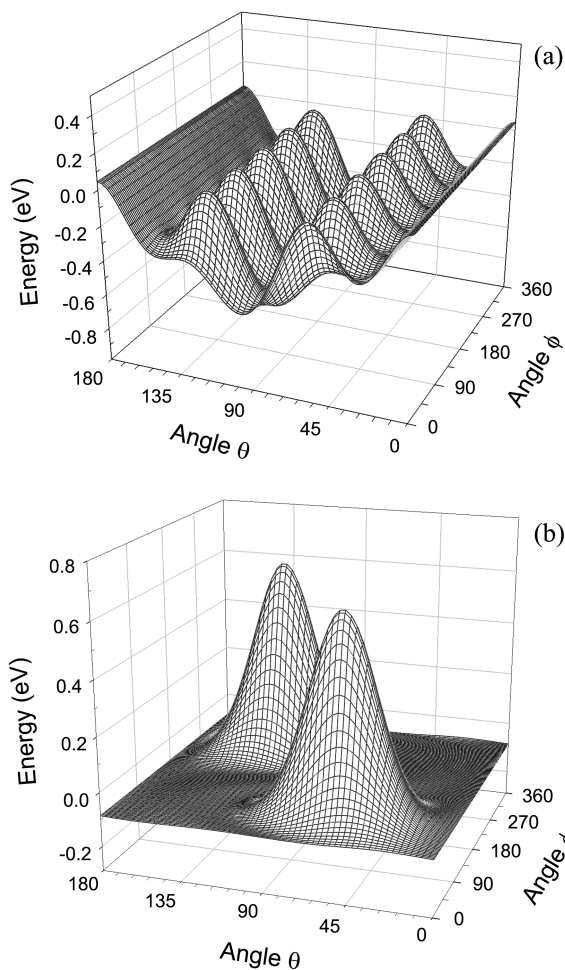


Figure 2. (a) Rotational potential energy surface for $(\text{Ar}_2^+) \text{Ar}_{12}$. The peak height is 0.0189 eV and lowest valley depth is -0.5478 eV. (b) Rotational potential energy surface for $(\text{Ar}_2^+) \text{Ar}_1$. The peak height is 0.6458 eV and lowest valley depth is -0.0840 eV.

strongly. Here $E_h = 0.363$ eV is the peak height measured from the valley. The frequency of the hindered motion is $\nu_h = (n/2\pi)(E_h/2I_{\text{Ar}_2^+})^{1/2} = 103 \text{ cm}^{-1}$, where $n = 5$ and $I_{\text{Ar}_2^+}$ is the moment of inertia of the ion. As θ approaches 90° , the interaction energy tends to the valley floor (-0.5478 eV). The perspective view between $\theta = 90^\circ$ and 180° illustrates the interaction of $\text{Ar}_{\text{ion(2)}}$ with Ar(7), Ar(8), ..., Ar(11) in the lower hemisphere. For comparison, we show the rotational PES for the one host atom case $(\text{Ar}_2^+) \text{Ar}$, where only two repulsive peaks (0.646 eV at $\theta = 57^\circ$, $\phi = 72^\circ$ and at $\theta = 122^\circ$, $\phi = 252^\circ$) are present; see Figure 2(b). Here we consider the host atom Ar(2), but any other host atom results in the same topology except that the two peaks are oriented differently on the θ - ϕ plane.

Equations of Motion. The equations of motion needed to solve for the time evolution of atom-atom distances and angles in the cluster $(\text{Ar}_2^+) \text{Ar}_{12}$ are

$$m_{\text{Ar}_2} d^2 \delta / dt^2 = -\partial V(r, \theta, \phi, \delta, \{q\}) / \partial \delta \quad (7-1)$$

$$\mu_{\text{Ar}_2} d^2 r / dt^2 = -\partial V(r, \theta, \phi, \delta, \{q\}) / \partial r \quad (7-2)$$

$$I_{\text{Ar}_2^+} d^2 \theta / dt^2 = -\partial V(r, \theta, \phi, \delta, \{q\}) / \partial \theta \quad (7-3)$$

$$I_{\text{Ar}_2^+} d^2 \phi / dt^2 = -\partial V(r, \theta, \phi, \delta, \{q\}) / \partial \phi \quad (7-4)$$

$$m_{\text{Ar}} d^2 q_n / dt^2 = -\partial V(r, \theta, \phi, \delta, \{q\}) / \partial q_n, n = 1-12 \quad (7-5)$$

where $\mu_{\text{Ar}_2^+}$ is the reduced mass of the ion and $m_{\text{Ar}_2} = 2m_{\text{Ar}}$. We take a sample size of 5000 trajectories and integrate the equations of motion for 5 nanoseconds. Initial vibrational energies of Ar_2^+ correspond to the quantum values of $3/2\hbar\omega$, $5/2\hbar\omega$, $7/2\hbar\omega$ and $9/2\hbar\omega$, which will be referred to $\nu = 1, 2, 3$ and 4, respectively. Numerical procedures using the standard routines based on the Adams-Moulton method²⁹ and random-sampling of initial conditions for r, θ, ϕ and $\{q\}$ are given in ref. 21.

Local translation mediates energy flow from vibration and rotation to host atoms, the process which can lead to fragmentation of $(\text{Ar}_2^+) \text{Ar}_{12}$. The rotation PES shown in Figure 2(a) indicates that the *ion-h* attraction dominates in the valleys between steeply rising peaks. The ion tends to travel along the attractive-interaction region undergoing an oscillatory motion. The motion describing the oscillatory behavior can be determined from the orientation-average of Eq. (1), which can be converted to a quadratic form to represent the oscillatory motion: $\langle V(\delta) \rangle = \langle V(0) \rangle + \frac{1}{2} \langle \partial^2 V(\delta) / \partial \delta^2 \rangle_0 \delta^2$, where the second derivative is evaluated at $r = r_e, \{q\} = 0$ and $\delta = 0$. The solution of the equation of local translation described by the quadratic function gives³⁰

$$\begin{aligned}
 \delta(t_0) = & \{2[E - \langle V(0) \rangle] / \langle \partial^2 V(\delta) / \partial \delta^2 \rangle_0\}^{1/2} \\
 & \times \ell \cos[(\langle \partial^2 V(\delta) / \partial \delta^2 \rangle_0 / m_{\text{Ar}})^{1/2} t_0 / \ell] \quad (8-1)
 \end{aligned}$$

$$\begin{aligned}
 [d\delta(t) / dt]_{t=t_0} = & -[2(E - \langle V(0) \rangle) / m_{\text{Ar}}]^{1/2} \\
 & \times \sin[(\langle \partial^2 V(\delta) / \partial \delta^2 \rangle_0 / m_{\text{Ar}})^{1/2} t_0 / \ell] \quad (8-2)
 \end{aligned}$$

Where E is the energy of collision between the ion and host atoms.

Results and Discussion

Energy Relaxation. The solution of the equations of motion given above for the total interaction energy describes how the local translation, rotation and vibration of the ion, ion...host and host-host distances evolve with time, and, in particular, their asymptotic behaviors at $t \rightarrow +\infty$. Before discussing the time evolution, we examine the dominant vibrations in the cluster; see Figure 3, where the Fourier transforms of the temporal development of q_n , δ and ion bond distance are shown. The host vibration is significantly structured between 15 and 60 cm^{-1} , the main peak appearing at 33 cm^{-1} . We note the presence of many other frequencies for the vibrations of host atoms; the peak shown here is a representative of them. The well-defined frequency of local translation obtained from the Fourier transform of the time dependence of δ is 121 cm^{-1} , which is close to $\nu = [|\partial^2 \langle V(\delta) \rangle / \partial \delta^2|_0 / m]^{1/2} / 2\pi = 127^{-1}$ obtained from Eq. (8-1). Also shown in Figure 3 is the 303 cm^{-1} peak for the embedded ion, which is red-shifted slightly from the fundamental 307 cm^{-1} of the free ion.²² Although not shown in Figure 3, we note the presence of yet another low frequency mode, the hindered rotational motion of a frequency 103 cm^{-1} . Thus the cluster is filled with low-frequency modes, the collection of which plays an essential role in promoting the vibrational relaxation of embedded ion and in turn, fragmentation of host atoms.

We now show the time evolution of intra-cluster motions. Figure 4(a) displays several trajectories representing short-time events occurring at 300 K for $\nu = 1$. Host atoms dissociating during the very early period are presented by trajectory A. Some host atoms dissociate after a short period of large amplitude motion (see C and D). Also shown is a representative of nondissociating events for comparison: see trajectory E. The time evolution of trajectory B is particularly interesting. For a clearer presentation, we reproduce it on an

expanded scale; see Figure 4(b). After some irregular motion during a very early period, the atom jumps to another site for a brief residency of ~ 70 ps, during which it performs a large amplitude oscillation before dissociating at $t \approx 100$ ps. The $Ar_2^+ - Ar(n)$ distance of this transient state is close to twice the first-neighbor Ar-Ar distance, suggesting the formation of a second shell site for a brief period. We find that a significant number of trajectories undergo such site-hopping before fragmentation, while others lead to direct fragmentation as shown by trajectories A, C and D.

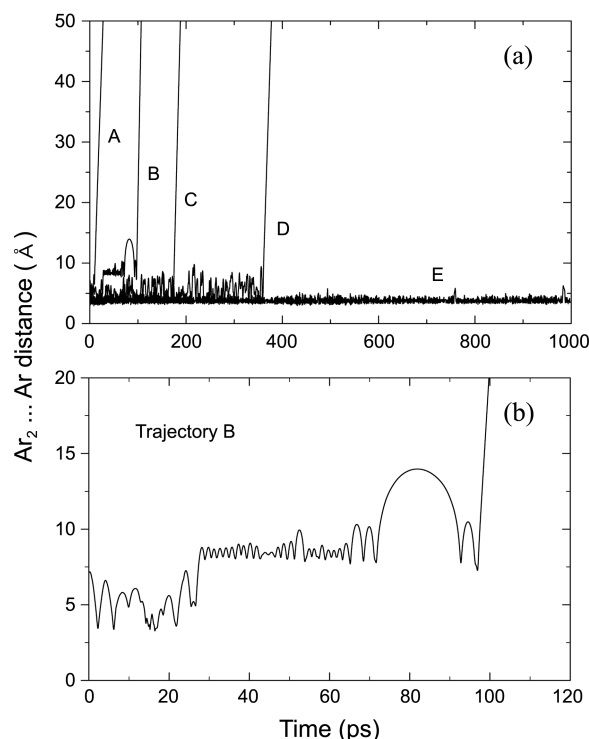


Figure 4. (a) Time evolution of *ion-h* distances for trajectories representing dissociative (A-D) and nondissociative (E) events for Ar_2^+ ($\nu = 1$) at 300 K. (b) Plot of trajectory B on an expanded scale.

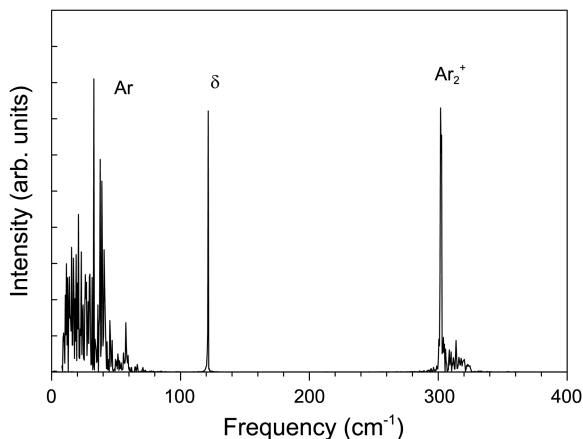


Figure 3. Power spectra of $(Ar_2^+)Ar_{12}$ for Ar vibration (highest peak 33 cm^{-1}), local translation (121 cm^{-1}) and embedded Ar_2^+ (highest peak 303 cm^{-1}).

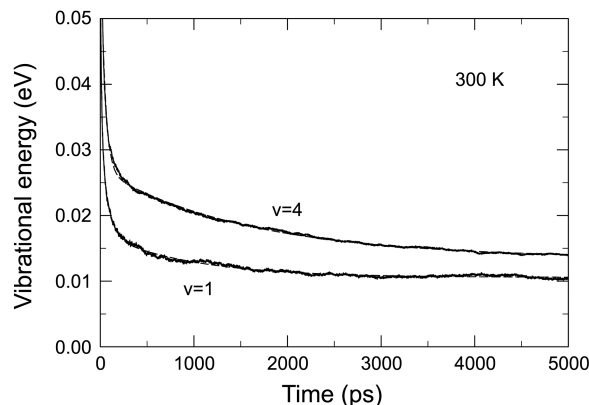


Figure 5. Time dependence of the vibrational energy of Ar_2^+ in $(Ar_2^+)Ar_{12}$ at 300 K for $\nu = 1$ and 4. The tri-exponential fitting curve for each case is shown by a dashed line, but the plot is not clearly seen as it overlaps nearly perfectly with the solid curve.

The ensemble-averaged energy transfer to host atoms closely fits the triple-exponential decay expression $\langle E_\nu(t) \rangle = c_0 + \sum_{n=1}^3 c_n \exp(-k_n t)$, where for example, for the ion in $\nu = 1$ at 300 K shown in Figure 5, $c_0 = 0.0106$ eV, $c_1 = 0.0266$ eV, $c_2 = 0.0172$ eV, $c_3 = 0.0067$ eV, $k_1 = 0.101$ ps $^{-1}$, $k_2 = 0.014$ ps $^{-1}$ and $k_3 = 1.05$ ns $^{-1}$. A tri-exponential form is needed to describe a rapid decrease in the energy during the early period of interaction and a slow variation toward the limiting value at a long time (>1 ns). The relaxation rate constants k_1 and k_3 represent these short and long timescales of energy transfer process; i.e., $k_1^{-1} \approx 10$ ps, whereas $k_3^{-1} \approx 1$ ns, respectively. The intermediate timescale $k_2^{-1} \approx 70$ ps represents the period immediately following the early drop of vibrational energy, so it can be considered as part of the lower end of the short timescale. The energy $c_0 = 0.0106$ eV is the amount left in the ion in the limit $t \rightarrow \infty$ and is about half the zero-point energy 0.0190 eV of Ar_2^+ in the present quasi-classical calculation. For $\nu = 4$ also at 300 K, the vibrational energy tends to the limiting value $c_0 = 0.0135$ eV, more rapidly than the $\nu = 1$ case. Energy flow is shown to be still very active beyond 1 ns. In fact, local translation

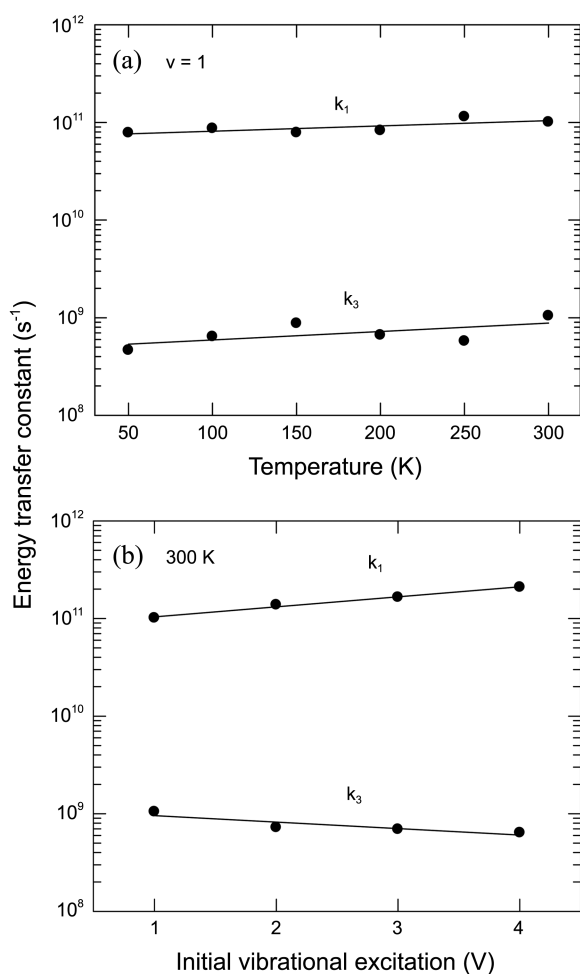


Figure 6. (a) Temperature dependence of short- and long-time relaxation rate constants (k_1 , k_3) for the core ion Ar_2^+ ($\nu = 1$) embedded in $(\text{Ar}_2^+)\text{Ar}_{12}$. (b) Dependence of short- and long-time relaxation rate constants on initial vibrational excitation of the core ion Ar_2^+ (ν) at 300 K.

continues to pump vibrational energy even after time as long as 3 ns, when energy flow is no longer active in the low vibrational excitation case of $\nu = 1$.

Figure 6(a) shows the temperature dependence of the relaxation rate constants. The value of k_1 increases only slightly from 7.83×10^{10} at 50 K to 1.01×10^{11} s $^{-1}$ at 300 K. Similarly, the long-time constant k_3 increases from 4.64×10^8 s $^{-1}$ at 50 K to 1.05×10^9 s $^{-1}$ at 300 K. The temperature dependence is weak in each case, but the scales of short- and long-time energy relaxation processes differ by two orders of magnitudes. The effects of initial vibrational excitation on energy transfer at 300 K shown in Figure 6(b) are not significant. At 300 K, the rate constants vary weakly with the vibrational excitation of Ar_2^+ , also showing the long-time process is slower than the short-time event by two orders of magnitude. A negative dependence of k_3 on the initial vibrational energy results from the difficulty of transferring the last trace of vibrational energy from the highly excited ion to local translation.

Fragmentation. In the cage environment, local translation causes the embedded ion to collide continuously with host atoms which oscillate around their equilibrium positions. The energy released by the excited Ar_2^+ and thermal energy of local translation lead to the fragmentation of host atoms, which oscillate around their equilibrium positions. The fragmentation process can then be analyzed in terms of the time evolution of the distance between the host atom and the *c.m.* of the embedded ion; see Figure 4(a). The extent of host atoms dissociated from 5000 $(\text{Ar}_2^+)\text{Ar}_{12}$ clusters with Ar_2^+ ($\nu = 1$) increases from 25% at 50 K only slightly to 29% at 300 K. For $\nu = 4$, where a greater amount of vibrational energy is released to host atoms, the extents at 50 and 300 K are 39 and 43%, respectively. The axial atoms Ar(6) and Ar(12) positioned on the *Z* axis dissociate much more readily than others. At 300 K, 77 and 96% of Ar(6) and Ar(12) of clusters with Ar_2^+ ($\nu = 1$) dissociate, respectively, whereas fragmentation is significantly less for layer atoms. In the lower layer, the extent of fragmentation sequentially decreases from 85% for Ar(11), 48% for Ar(10), 18% for Ar(9), 5% for Ar(8) and 1% for Ar(7). On the other hand, the extent of fragmentation of host atoms in the upper layer is very low, the percentages being 13% for Ar(5) and only 2% of Ar(4). The host atoms Ar(3), Ar(2) and Ar(1) do not dissociate at all.

The above numbers indicate the extent of fragmentation from the lower hemisphere is nearly three times that from the upper hemisphere in the model shown in Figure 1. The extent of fragmentation is nearly independent of temperature and vibrational excitation. The most frequently dissociating atoms are the two axial atoms and Ar(10) and Ar(11). Further, these atoms dissociate on a short-time scale characterized by the k_1^{-1} timescale discussed above. For example, 65% of dissociative events of Ar(12) in 5000 $(\text{Ar}_2^+)\text{Ar}_{12}$ with Ar_2^+ ($\nu = 1$) at 300 K occur within 100 ps from the start of *ion-h* interaction. Only 6% dissociate in 2 to 5 ns. As the initial burst of fragmentation consumes most of the available energy, the remaining bound atoms have a difficulty in

gaining energy from various low frequency motions, thus taking a longer time to dissociate or do not dissociate at all. The most important mode of fragmentation is due to the energy flow from the embedded ion sequentially to host atoms Ar(11), Ar(10), Ar(9), Ar(8) and Ar(7) *via* the apex atom Ar(12), where collective motions of all lower-layer atoms facilitate energy flow and fragmentation induced by the apex atom. The apex atom Ar(6) also initiates a fragmentation string in the upper layer but its effect does not propagate long. This result leads to the formation of intermediate-sized clusters mainly composed of (undissociated) layer atoms in a short-time period. We note that when the icosahedron sketched in Figure 1 is rotated by 180° in the θ direction, Ar(1), Ar(2), ..., Ar(6) now form the lower hemisphere, but the same fragmentation pattern is found as renaming the axes or renumbering host atoms does not lead to a different configuration. In fact, any host atom and its five nearest neighbors in an icosahedron form a hemisphere. The important point to be made is that fragmentation occurs efficiently from one hemisphere over the other *via* a chain of consecutive events from axial to layer atoms. For a fixed cluster structure, there are thus preferred sites and pathways of fragmentation facilitated by collective motions of the host atoms in one of the hemispheres at and below room temperature.

Figure 7 shows that the principal fragmentation products of $(\text{Ar}_2^+)\text{Ar}_{12} \rightarrow (\text{Ar}_2^+)\text{Ar}_n + (12-n)\text{Ar}$ are clusters with n between 7 and 10, the distribution peaking at $n = 9$ for $\nu = 1$. For $\text{Ar}_2^+(\nu = 1)$ at 300 K, 29% of host atoms dissociate as mentioned above, leaving 71% of them intact at various sites in the cluster. The majority of these bound atoms is in the $n = 10, 9$ and 8 clusters. The distribution of cluster sizes shown in Figure 7 is the number of $(\text{Ar}_2^+)\text{Ar}_n$ clusters divided by the total number of $(\text{Ar}_2^+)\text{Ar}_{12}$ sampled. The distribution curve for $\text{Ar}_2^+(\nu = 1)$ at 300 K is peaked at the size 9 or $(\text{Ar}_2^+)\text{Ar}_9$. The distribution for the same vibrational excitation at 50 K is very similar to that at 300 K. Below $n = 8$, the probability decreases rapidly with decreasing cluster size.

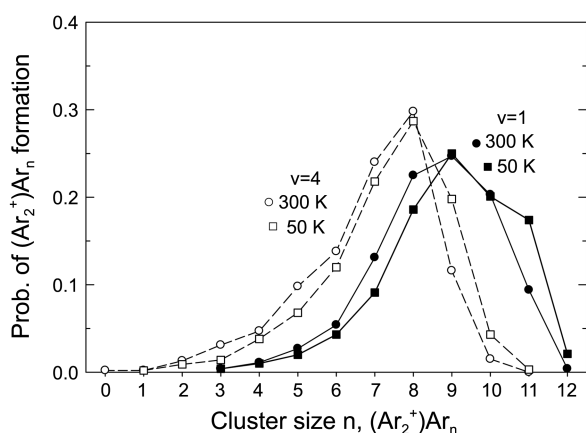


Figure 7. Dependence of the fragmentation probability on cluster size for $(\text{Ar}_2^+)\text{Ar}_n$. For initial excitation $\nu = 1$; filled circles with solid lines are at 300 K and filled squares with solid lines are at 50 K. For initial excitation $\nu = 4$: open circles with dashed lines are at 300 K and open squares with dashed lines are at 50 K.

As noted above, after several host atoms dissociate, the available energy remaining in the cluster is low, so further dissociation forming smaller clusters becomes increasingly difficult. In fact, no clusters with $n = 1$ and 2 are found in all cases shown in Figure 7. The figure also shows that the number of undissociated clusters $(\text{Ar}_2^+)\text{Ar}_{12}$ is negligible, the probabilities being only 0.004 and 0.021 at 300 and 50 K, respectively. When the embedded ion is excited to $\nu = 4$, the amount of energy transfer to host atoms is significantly larger than the low excitation case (see Figure 5) and the probability peak shifts downward with the dominant products being $(\text{Ar}_2^+)\text{Ar}_7$ and $(\text{Ar}_2^+)\text{Ar}_8$; see Figure 7 for the $\nu = 4$ curves at 300 and 50 K. The size distribution shows that $n = 12$ and 11 clusters are now absent, while small but noticeable probabilities are found for $n = 1$ and 2, which reflects host atoms have difficulty of gaining the last trace of energy for dissociation, as noted in Figure 6(b). For example, the probability of producing $(\text{Ar}_2^+)\text{Ar}_{10}$ for $\nu = 4$ at 300 K is only 0.015, far less than the $\nu = 1$ probability 0.20, whereas the probabilities for small clusters such as $(\text{Ar}_2^+)\text{Ar}_2$ are 0.013 and 0. Although their curves are not shown, we note that the cluster size distribution for $\nu = 2$ and 3 takes intermediate positions between the $\nu = 1$ and 4 curves shown in Figure 7.

Conclusions

We report the results of dynamics of intra-cluster energy flow and fragmentation of icosahedral $(\text{Ar}_2^+)\text{Ar}_{12}$ with a vibrationally excited core ion over the temperature range of 50-300 K. The time evolution of vibrational energy transfer calculated in classical mechanics procedures using an analytic representation of the many-body interaction potential can be fit closely to a tri-exponential expression, which shows energy relaxation taking place over a wide range of time. The main portion of the vibrational energy of Ar_2^+ flows to host atoms *via* local translation on a picosecond scale and leads to fragmentation of the cluster. The dependence of relaxation rate constants on temperature and initial vibrational excitation of the diatomic ion is not strong.

About one-quarter of $(\text{Ar}_2^+)\text{Ar}_{12}$ with the ion in $\nu = 1$ are found to fragment into various sizes in the temperature range 50-300 K. The extent of fragmentation nearly doubles for the ion in $\nu = 4$. The size distribution of fragmentation products is peaked for $(\text{Ar}_2^+)\text{Ar}_9$ for $\nu = 1$ and is nearly independent of temperature. The peak shifts to $(\text{Ar}_2^+)\text{Ar}_8$ for $\nu = 4$. The overall feature of size distribution varies significantly as vibrational excitation increases. Nearly all axial atoms Ar(6) and Ar(12) dissociate within a short-time period of ~ 100 ps. Further fragmentation is dominated sequentially by the layer atoms in one hemisphere of the icosahedron over another, which is a sign of regioselectivity showing the preference of energy flow in one region over all others. Thus efficient pathways of fragmentation in the vibrationally excited ion-embedded cluster appear to be collective motions of nearest host atoms surrounding the apex site induced by the local translation of the core ion.

Acknowledgments. J. R. gratefully acknowledges the financial support from Chonnam National University.

References

1. Woodward, C. A.; Upham, J. E.; Stace, A. J.; Murrell, J. N. *J. Chem. Phys.* **1989**, *91*, 7612.
2. Tanner, G. M.; Bhattacharya, A.; Nayak, S. K.; Mahanti, S. D. *Phys. Rev. E* **1997**, *55*, 322.
3. Böhmer, H.-U.; Peyerimhoff, S. D. *Z. Phys. D-Atoms, Molecules and Clusters* **1989**, *11*, 239.
4. Snodgrass, J. T.; Roehl, C. M.; Bowers, M. T. *Chem. Phys. Lett.* **1989**, *159*, 10.
5. Hiraoka, K.; Mori, T. *J. Chem. Phys.* **1989**, *90*, 7143.
6. Gadea, F. X.; Savrda, J.; Paidarova, I. *Chem. Phys. Lett.* **1994**, *223*, 369.
7. Gadea, F. X.; Paidarova, I. *Chem. Phys.* **1996**, *209*, 281.
8. Doltsinis, N. L.; Knowles, P. J. *Mol. Phys.* **1998**, *94*, 981.
9. Doltsinis, N. L.; Knowles, P. J.; Naumkin, F. Y. *Mol. Phys.* **1999**, *96*, 749.
10. Ming, L.; Markovic, N.; Svanberg, M.; Pettersson, J. B. C. *J. Phys. Chem. A* **1997**, *101*, 4011.
11. Froudakis, G. E.; Fanourgakis, G. S.; Farantos, S. C.; Xantheas, S. S. *Chem. Phys. Lett.* **1998**, *294*, 109.
12. Greenblatt, B. J.; Zanni, M. T.; Neumark, D. M. *J. Chem. Phys.* **1999**, *111*, 10566.
13. Hrivnak, D.; Kalus, R. *Chem. Phys.* **2001**, *264*, 319.
14. Barat, M.; Brenot, J. C.; Fayetteon, J. A.; Picard, Y. *J. Chem. Phys.* **2002**, *117*, 1497.
15. Ismail, I. M.; Lepere, V.; Barat, M.; Fayetteon, J. A.; Picard, Y. J.; Wohrer, K. *J. Chem. Phys.* **2006**, *124*, 164305.
16. Lepere, V.; Picard, Y. J.; Barat, M.; Fayetteon, J. A.; Lucas, B.; Beroff, K. *J. Chem. Phys.* **2009**, *130*, 194301.
17. Ritschel, T.; Zuhrt, C.; Zülicke, L.; Kuntz, P. J. *Eur. Phys. J. D* **2007**, *41*, 127.
18. da Silva, F. F.; Bartle, P.; Denifl, S.; Echt, O.; Mark, T. D.; Scheier, P. *Phys. Chem. Chem. Phys.* **2009**, *11*, 9791.
19. Shin, H. K. *J. Chem. Phys.* **2011**, *134*, 124301.
20. Wüest, A.; Merkt, F. *J. Chem. Phys.* **2004**, *120*, 638.
21. Shin, H. K. *J. Chem. Phys.* **2010**, *132*, 104302.
22. Signorell, R.; Wüest, A.; Merkt, F. *J. Chem. Phys.* **1997**, *107*, 10819.
23. Moseley, J. T.; Saxon, R. P.; Huber, B. A.; Cosby, P. C.; Abouaf, R.; Tadjeddine, M. *J. Chem. Phys.* **1977**, *67*, 1659.
24. Aziz, R. A.; Chen, H. H. *J. Chem. Phys.* **1977**, *67*, 5719.
25. Aziz, R. A. *J. Chem. Phys.* **1993**, *99*, 4518.
26. Dehmer, P. M.; Dehmer, J. L. *J. Chem. Phys.* **1978**, *69*, 125.
27. Herman, P. R.; LaRocque, P. E.; Stoicheff, B. P. *J. Chem. Phys.* **1988**, *89*, 4535.
28. Bell, R. J.; Kingston, A. E. *Proc. Phys. Soc.* **1966**, *88*, 901.
29. MATH/LIBRARY, *Fortran Subroutines for Mathematical Applications*, Version 2.0 (IMSL, Houston, 1991), pp. 755-771 for DIVPAG to solve an initial-value problem for ordinary differential equations using Adams-Moulton's method and pp. 1319-1320 for DRNUN to generate random numbers from flat (0,1) distributions.
30. Shin, H. K. *Chem. Phys. Lett.* **1974**, *26*, 450; see Eqs. 7 and 8.